Transport properties of the layered Zintl compound $SrZnSb_2$

Andrew F. May,[1,a] Eric S. Toberer,[2] and G. Jeffrey Snyder[2]
[1]*Chemical Engineering, California Institute of Technology, 1200E. California Blvd., Pasadena, California 91125, USA*
[2]*Materials Science, California Institute of Technology, 1200 E. California Blvd., Pasadena, California 91125, USA*

(Received 16 April 2009; accepted 30 May 2009; published online 9 July 2009)

Transport properties of the layered Zintl compound $SrZnSb_2$ have been characterized from room temperature to 725 K on polycrystalline samples. $SrZnSb_2$ samples were found to be *p*-type with a Hall carrier concentration of 5×10^{20} cm^{-3} at room temperature, and a small Seebeck coefficient and electrical resistivity are observed. A single band model predicts that, even with optimal doping, significant thermoelectric performance will not be achieved in $SrZnSb_2$. A relatively low lattice thermal conductivity is observed, $\kappa_L\sim1.2$ W m^{-1} K^{-1}, at room temperature. The thermal transport of $SrZnSb_2$ is compared to that of the layered Zintl compounds AZn_2Sb_2 (A=Ca, Yb, Sr, Eu), which have smaller unit cells and larger lattice thermal conductivity, $\kappa_L\sim2$ W m^{-1} K^{-1}, at 300 K. Ultrasonic measurements, in combination with kinetic theory and the estimated κ_L values, suggest that the lower κ_L of $SrZnSb_2$ is primarily the result of a reduction in the volumetric specific heat of the acoustic phonons due to the increased number of atoms per unit cell. Therefore, this work recommends that unit cell size should be considered when selecting Zintl compounds for potential thermoelectric application. © *2009 American Institute of Physics*. [DOI: 10.1063/1.3158553]

I. INTRODUCTION

The search for high efficiency thermoelectric materials encompasses many classes of semiconductors. While most conventional thermoelectric materials employ tellurium, its low natural abundance suggests that the discovery of non-Te based thermoelectric materials may be required for widespread application. Also necessary is high thermoelectric conversion efficiency, which is characterized (at the material level) by the figure of merit, $zT=\alpha^2T/\rho\kappa$, where α is the Seebeck coefficient, ρ is the electrical resistivity, and the thermal conductivity κ is the sum of the electronic κ_e and lattice κ_L contributions. In general, large zT is difficult to obtain due to the coupling of these transport properties via carrier concentration n and temperature T.

Zintl compounds are attractive for thermoelectric application due to their valence-precise nature, which frequently results in tunable semiconductors.[1,2] Also, Zintl compounds are often composed of discrete structural units (layers, cages, channels, and polyanionic groups) that promote low κ_L.[3–6] Many material systems fall into the Zintl formalism and several have demonstrated large thermoelectric efficiency, including $Yb_{14}MnSb_{11}$, $Ba_8Ga_{16}Ge_{30}$, and the filled $CoSb_3$.[6] However, the transport properties of many Zintl compounds remain uncharacterized.

Here, we report on the electrical and thermal transport properties of polycrystalline $SrZnSb_2$ from room temperature to 725 K. $SrZnSb_2$ was previously predicted to be a semimetal by *ab initio* calculations, and a maximum zT of 0.14 (0.21) was estimated for *p*-type (*n*-type) conduction at 300 K.[7] The crystal structure of $SrZnSb_2$ [orthorhombic, *Pnma*; Fig. 1(a)] is derived from the $ThCr_2Si_2$ structure (tetragonal, $I4/mmm$), where anionic slabs of edge sharing tetrahedra are separated by square monolayers of cations. In $SrZnSb_2$, every other $(Zn_2Sb_2)^{2-}$ slab is replaced by a monolayer consisting of $(Sb_2)^{2-}$ zig zag chains.

To gain insights into the relationship between crystal structure and transport properties in Zintl compounds, the data obtained for $SrZnSb_2$ are compared to those of the layered AZn_2Sb_2 (A=Ca, Yb, Sr, Eu) Zintl compounds. The latter compounds have been shown to possess moderate thermoelectric performance, with $0.5\leqslant zT\leqslant1$ at 750 K.[8,9] As shown in Fig. 1(b), the AZn_2Sb_2 compounds ($P\bar{3}m$ $CaAl_2Si_2$ parent compound) have structural features similar to $SrZnSb_2$, but the unit cell of $SrZnSb_2$ is larger due to the layer of $(Sb_2)^{2-}$ zig zag chains. The AZn_2Sb_2 (A=Ca, Yb, Sr, Eu) compounds are composed of trigonal monolayers of A^{2+} cations separating $(Zn_2Sb_2)^{2-}$ slabs. The

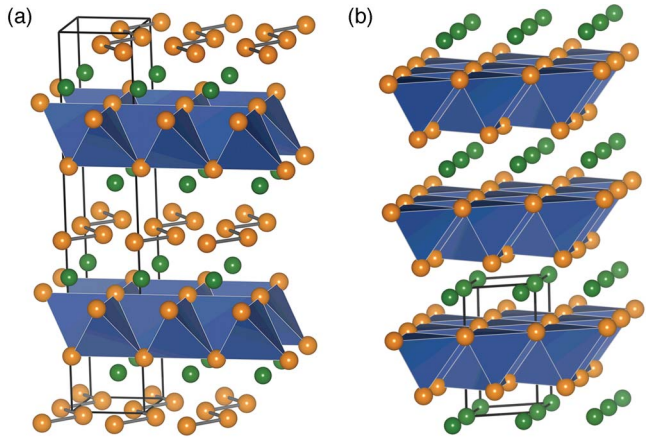

FIG. 1. (Color online) Crystal structures of (a) $SrZnSb_2$ and (b) $SrZn_2Sb_2$ with unit cells outlined in black. Green spheres represent Sr, gold sphere represents Sb, and Zn is located within the tetrahedrons.

[a]Electronic mail: may@caltech.edu.

anionic slabs can be viewed as two puckered graphitic Sb–Zn layers which have been brought into contact.[10]

II. METHODS

A. Synthesis

Stoichiometric amounts of the elements (at least 99.9% metal basis purity) were combined in a pyrolitic BN crucible, which was sealed in a quartz tube evacuated to 1×10^{-5} torr. Samples were slowly heated from 575 to 1225 K, and the resulting melt was held at 1225 K for 30 min. The melt was cooled to 825 K in 2.5 h, and the sample was annealed at 825 K for 2.5 h. The resulting ingot was ball milled under argon for 15 min in the high energy SPEX 8000 Series Mixer/Mill utilizing stainless steel vial and balls. The fine grain, homogeneous powder obtained from milling was hot pressed in a high-density graphite die (POCO) at 825 K, for approximately 3 h, while roughly 1.4 metric ton of force was placed on a 12 mm diameter surface. The dense ingots obtained from hot pressing were cut using a slow cut saw with nonaqueous lubricant, and the resulting wafers were ~1–2 mm thick.

B. Characterization

X-ray diffraction was performed on powder samples via a Phillips X'Pert plus diffractometer using Cu $K\alpha$ radiation. Transport data were collected between 300 and 725 K while under dynamic vacuum. A constant ΔT of ~10 K was utilized to obtain Seebeck coefficients by measuring voltage via Nb wires and T at the corresponding chromel-Nb junctions. The van der Pauw method was utilized to obtain the Hall density ($n_H = 1/R_H$, where R_H is the Hall coefficient) and electrical resistivity; a magnetic field of 2 T and currents of 500 mA were utilized. A Netzsch LFA 457 measured the thermal diffusivity, and heat capacity is estimated by the method of Dulong–Petit. Shear and longitudinal sound velocities were measured at room temperature using a Panametrics NDT 5800 pulser/receiver and a Tektronix TDS 1012 digital oscilloscope with honey couplant.

III. RESULTS AND DISCUSSION

$SrZnSb_2$ samples were nearly phase pure with a high density (>97% theoretical). The presence of a small amount (1–2 wt %) of elemental Sb impurity is observed in the refinement of powder x-ray diffraction data.

A. Electrical transport

$SrZnSb_2$ was found to be a p-type conductor with a room temperature Hall carrier concentration (n_H) of 5×10^{20} cm^{-3}. As shown in Fig. 2, the value of n_H for $SrZnSb_2$ increases quickly with increasing temperature, which is indicative of a small band gap semiconductor or a semimetal. At high temperatures, the single-carrier description yields an exaggerated n_H due to the excitation of electrons into the conduction band. Without knowledge regarding the mobility of holes and electrons (as a function of temperature), it is impossible to calculate the true hole concentration and mobility at high T.

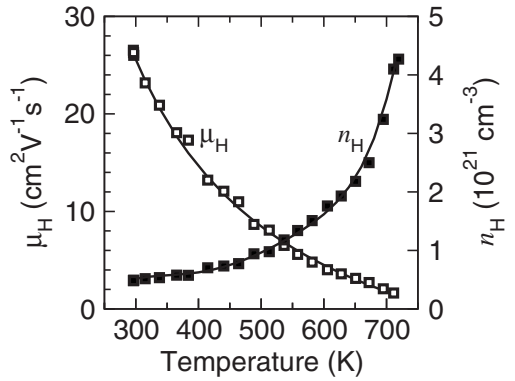

FIG. 2. The Hall carrier concentration (filled markers) and mobility (open markers) of $SrZnSb_2$ as a function of temperature. The smooth curves are guides to the eye.

The electrical resistivity (ρ) of $SrZnSb_2$ is small and increases with increasing temperature, as shown in Fig. 3. The temperature dependence of $SrZnSb_2$ is observed to be less than linear due to the thermal excitation of carriers. The corresponding Hall mobility (μ_H) decreases with increasing temperature (Fig. 2), presumably due to scattering by acoustic phonons, and at high temperatures multicarrier effects yield an underestimated μ_H.

Seebeck coefficient (α) measurements support p-type conduction, with positive α obtained for all temperatures (Fig. 3). The Seebeck coefficient of $SrZnSb_2$ is small, likely due to the high doping level, and the observed temperature dependence is similar to that of a heavily doped semiconductor. A thermal band gap of $E_g = 0.07$ eV is estimated using the maximum value of α and the corresponding T: $E_g \sim 2e\alpha_{max}T_{max}$.[11] The effective mass of $SrZnSb_2$ is estimated to be $0.92m_e$ at room temperature, where m_e is the free electron mass. The effective mass is calculated from the room temperature n_H and α using a single parabolic band model with carrier mobility assumed to be limited by acoustic phonon scattering.[12]

The transport properties of AZn_2Sb_2 (A = Sr, Ca, Yb, Eu) were previously reported and are summarized here.[8,9,13] The nominally stoichiometric compounds were found to be extrinsically doped, p-type semiconductors with 1.5×10^{19}–1.5×10^{20} holes/cm^3 at 300 K. Using the

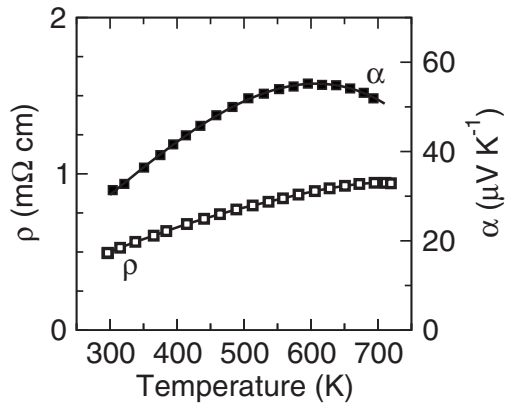

FIG. 3. Temperature dependence of the Seebeck coefficient (filled markers) and electrical resistivity (open markers) for $SrZnSb_2$.

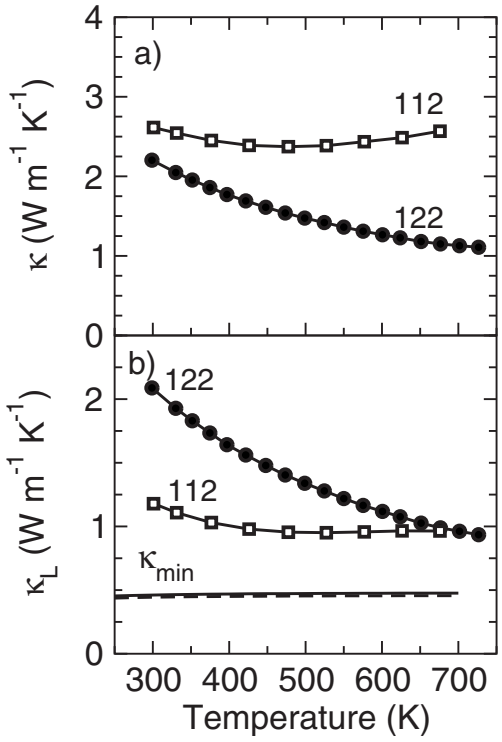

FIG. 4. (a) The total thermal conductivity of $SrZnSb_2$=112 is compared to that of $SrZn_2Sb_2$=122. (b) Estimation of the lattice thermal conductivity κ_L reveals lower κ_L in $SrZnSb_2$ than in $SrZn_2Sb_2$. Also shown is κ_{min} calculated via Cahill's representation, which is similar for both compounds. A contribution from the bipolar thermal conductivity is expected for $SrZnSb_2$ at high temperatures.

same approach as above, $E_g \sim 0.3$ eV and $m^* \sim 0.6m_e$ have been calculated for these compounds,[13] and we have calculated $m^*=0.57m_e$ at 300 K for $EuZn_2Sb_2$ from the data in Ref. 9. The carrier mobility of all AZn_2Sb_2 (A=Sr,Ca,Yb,Eu) is found to be larger than that in $SrZnSb_2$, probably due to the reduced effective mass and lower carrier density. While the AZn_2Sb_2 compounds have similar m^*, the variation in μ does not follow any trend with carrier concentration and the Yb and Eu compounds have surprisingly large μ. The difference in m^*, μ, and E_g between these compounds and $SrZnSb_2$ suggests that the layer of infinite Sb chains impacts the electronic structure of $SrZnSb_2$ near the top of the valence band.

B. Thermal transport

The thermal conductivity shown in Fig. 4(a) is calculated as the product of the density d, thermal diffusivity D_T, and heat capacity C_P, the latter of which is estimated using the method of Dulong–Petit. For $SrZnSb_2$ (112), C_P=0.252 J/g K and for $SrZnSb_2$ (112) C_P=0.270 J/g K. As seen in Fig. 4(a), the thermal conductivity of $SrZnSb_2$ is relatively independent of temperature. Specifically, the value of κ initially decreases with increasing temperature, and then rises for $T>500$ K. The lattice contribution shown in Fig. 4(b) is estimated by $\kappa_L=\kappa-\kappa_e$. The electronic contribution is obtained by the Wiedemann–Franz relationship, $\kappa_e=L\sigma T$, where the Lorenz number L is calculated using a single band model with carrier mobility limited by acoustic phonon scattering.[12] The calculation of L yields values between 2.35×10^{-18} and 2.19×10^{-8} W Ω K^{-2} for temperatures between 300 and 675 K, respectively.

The estimation of κ_L reveals a significant contribution to κ from κ_e, as expected for materials with low ρ. In Fig. 4(b), the value of κ_L for $SrZnSb_2$ is observed to decrease with increasing temperature up to roughly 500 K, where it remains at ~1 W/m K. A decrease in κ_L with increasing temperature is expected for crystalline materials (T^{-1} decay due to an increase in phonon-phonon scattering for the acoustic modes), while temperature independent κ_L is typically observed in disordered systems.

The plateau above 500 K does not suggest that $SrZnSb_2$ has a glasslike thermal conductivity at high T. At high temperatures κ_e possesses additional contributions due to the thermal excitation of charge carriers across the band gap. In particular, the bipolar thermal conductivity (κ_b) can occur when both holes and electrons are present (here we consider κ_b as one part of κ_e). The value of κ_b cannot be determined without knowledge on the electronic properties of both carrier types. We expect κ_b to be significant at high temperature in $SrZnSb_2$ due to the large increase in n_H, which suggests that holes and electrons are thermally activated. The net result is an overestimation of κ_L, particularly at high temperatures, and thus a temperature independent κ_L is observed as an artifact of the analysis.

As shown in Fig. 4(b), the lattice thermal conductivity of $SrZnSb_2$ (112) is roughly one-half that of $SrZn_2Sb_2$ (122) at 300 K. For most of the temperatures examined, κ_L for $SrZnSb_2$ is significantly lower than that of $SrZn_2Sb_2$. The values of κ_L converge at high T likely due to the crystalline-like decay (T^{-1}) of κ_L in $SrZn_2Sb_2$ and the presence of κ_b in $SrZnSb_2$. Due to the complexity of transport at high T in $SrZnSb_2$, we focus on the room temperature properties and highlight the differences between these materials. Furthermore, at room temperature we do not expect significant variation from the estimated values of C_P.

Speed of sound data are utilized to estimate the mean phonon group velocity (v_m), Debye temperature (Θ_D), and average acoustic phonon mean free path (l_{ac}), which are discussed below. The sample of $SrZn_2Sb_2$ utilized was synthesized in a manner similar to that described here for $SrZnSb_2$. The room temperature data are summarized in Table I, where

TABLE I. Room temperature properties of $SrZnSb_2$ and $SrZn_2Sb_2$.

Compound	n_a (atoms/cell)	κ_L (W/m K)	v_l (m/s)	v_t (m/s)	v_m (m/s)	Θ_D (K)	l_{ac} (Å)	C_{ac} (J/g K)
$SrZnSb_2$	16	1.2	3540	2040	2270	222	170	0.0157
$SrZn_2Sb_2$	5	2.1	3750	2010	2240	222	91	0.0540

it is shown that the two compounds have very similar v_m and Θ_D, which was estimated via

$$\Theta_D = \frac{v_m \hbar}{k_b}\left(\frac{6\pi^2}{V}\right)^{1/3}, \quad (1)$$

where V is the average volume per atom and v_m is calculated from the longitudinal v_l and transverse v_t speeds of sound via $v_m = 3^{1/3}(v_l^{-3} + 2v_t^{-3})^{-1/3}$.[14] The values of v_l and v_t are also used to estimate the minimum value of the thermal conductivity (κ_{min}) with Cahill's formulation for amorphous materials,[15]

$$\kappa_{min} = \left(\frac{\pi}{6}\right)^{1/3} k_b V^{-2/3} \sum_i v_i \left(\frac{T}{\Theta_i}\right)^2 \int_0^{\Theta_i/T} \frac{x^3 e^x}{(e^x - 1)^2} dx. \quad (2)$$

Within Cahill's model, both compounds are predicted to have very similar κ_{min} [lower curves in Fig. 4(b)], which is roughly one-half of the κ_L observed at high T. The values of V employed here are obtained from Refs. 16 and 17. In Eq. (2), the summation is over the one longitudinal and two transverse modes with $\Theta_i = v_i(\hbar/k_b)(6\pi^2/V)^{1/3}$. When utilizing Slack's formulation for κ_{min} (including the optical contribution),[18] a smaller $\kappa_{min} = 0.28$ W m^{-1} K^{-1} is calculated for $SrZnSb_2$, while $\kappa_{min} = 0.45$ W m^{-1} K^{-1} for $SrZn_2Sb_2$; the difference is due to a smaller acoustic contribution for $SrZnSb_2$ (related to the number of atoms per unit cell, discussed below).

When thermal transport is governed by acoustic phonons, such as implied by the temperature dependence of κ_L, it is perhaps more appropriate to consider average properties of the acoustic modes. The mean free path of acoustic phonons is then obtained from

$$\kappa_L = \tfrac{1}{3} dC_{ac} v_{ac} l_{ac}, \quad (3)$$

where $dC_{ac} = dC_P/n_a$ is the contribution of the acoustic phonons to the volumetric specific heat for a primitive cell containing n_a atoms, and $v_{ac} = v_m$. From this formulation, and the summary of results in Table I, it is readily observed that $(dC_{ac})_{SrZnSb_2}/(dC_{ac})_{SrZn_2Sb_2} \sim 0.3$, while $l_{ac,SrZnSb_2}/l_{ac,SrZn_2Sb_2} \sim 1.9$, and thus the reduced κ_L in $SrZnSb_2$ is associated with a decrease in the ability of acoustic phonons to carry heat. Note that if the classic definition of the average phonon mean free path is utilized (C_P in place of C_{ac}), the average mean free path of $SrZnSb_2$ would be roughly a factor of 2 smaller than that of $SrZn_2Sb_2$ and both mean free paths would be roughly an order of magnitude smaller than those reported in Table I.

From a structural point of view, the larger unit cell of $SrZnSb_2$ results in reduced κ_L via a reduction in the volumetric specific heat of heat carrying phonons. According to Slack, when only acoustic phonons contribute to the thermal transport, the thermal conductivity at Θ_D can be estimated by

$$\kappa_L = \frac{B\bar{M}V^{1/3}\Theta_D^2}{n_a^{2/3}\gamma^2}, \quad (4)$$

where $\bar{M}$ is the average atomic mass, γ is the Grüneisen parameter, and the constant $B = 3.04 \times 10^7$ s^{-3} K^{-3} for $\gamma = 2$.[19] The trends observed here are in agreement with the theoretical prediction provided γ does not vary much between the two compounds. Specifically, when $\gamma = 2$ is assumed, Eq. (4) yields $\kappa_L = 1.78$ W m^{-1} K^{-1} for $SrZnSb_2$ and $\kappa_L = 3.56$ W m^{-1} K^{-1} for $SrZn_2Sb_2$. The main difference is the value of n_a $(n_{a,SrZnSb_2}/n_{a,SrZn_2Sb_2})^{-2/3} = (16/5)^{-2/3} = 0.46$, and thus unit cell size can explain the trends in κ_L observed here.

The role of optical phonons complicates this comparison some, as the increased number of atoms per unit cell in $SrZnSb_2$ leads to more optical modes than in $SrZn_2Sb_2$. Optical phonons may carry heat; however, in these compounds the mass ratios are greater than 1 (between 1.3 and 1.9) and thus optical modes are not expected to contribute significantly to thermal transport.[19] Also, optical modes can promote thermal resistance through the annihilation of acoustic phonons: acoustic + acoustic → optic.[20] Therefore, the small amount of heat carried by the optical phonons may be offset by an increased scattering of the acoustical modes.

Structural features must also be considered as a source for low κ_L in $SrZnSb_2$. The infinite chains of Sb may be flexible and/or have large thermal parameters that promote phonon scattering. Also, the similarity in a and b lattice parameters may allow the frequent production of twin boundaries, which would also promote phonon scattering. We do not believe that point defects (vacancies) associated with hole production are responsible for reduced κ_L in $SrZnSb_2$ because large changes in defect concentrations would be expected between $SrZn_2Sb_2$ and $YbZn_2Sb_2$ (based on the values of n_H), and these compounds have similar κ_L. The presence of Sb impurity in $SrZnSb_2$ is not believed to be the source of low κ_L as the $SrZn_2Sb_2$ samples contained a similar quantity of ZnSb impurity. Finally, the scattering of phonons via charge carriers was determined to be insignificant based on the theory by Ziman.[21,22] Furthermore, scattering effects are unlikely to be the source for reduced κ_L as l_{ac} for $SrZnSb_2$ is larger than l_{ac} for $SrZn_2Sb_2$, which suggests less phonon scattering in $SrZnSb_2$.

The data reported in Ref. 9 suggests a significantly lower κ_L for $EuZn_2Sb_2$ at high T. However, this is calculated using $L = 2.45 \times 10^{-8}$ W Ω K^{-2}, which is the metallic limit that generally overestimates κ_e. Using the same single band model discussed here, we estimate κ_L to be slightly lower in $EuZn_2Sb_2$ than in $SrZn_2Sb_2$: κ_L of $EuZn_2Sb_2$ ~ 1.8 W m^{-1} K^{-1} at 314 K and $\kappa_L \sim 0.7$ W m^{-1} K^{-1} at 713 K (these values correspond to $L = 1.82 \times 10^{-8}$ and 1.65×10^{-8} W Ω K^{-2}, respectively).

C. Thermoelectric performance

The zT of $SrZnSb_2$ reaches a maximum of 0.09 at 625 K, and the doping level is too large for optimum performance. By computing $\beta = \mu_0 m^{*3/2}(T/300)^{5/2}/\kappa_L$ for an unoptimized sample, the optimum zT can be predicted using a single band model (we assume that the carrier mobility is limited by acoustic phonon scattering).[23] The calculation of zT predicts a maximum zT of 0.15 for $n = 2.8 \times 10^{19}$ holes cm^{-3} at 300 K and a zT of 0.3 at 500 K for $n = 9.8 \times 10^{19}$ holes cm^{-3}. The estimates of maximum zT at room temperature are consistent with *ab initio* predictions, which suggested that a zT of 0.14 was obtainable for p-type compositions at 300 K.[7] At 500 K,

$zT=0.3$ is likely to be difficult to achieve due to the detrimental effects of minority carriers, which are more readily observed at low carrier concentrations and small E_g. Thus $SrZnSb_2$ is not a viable candidate for thermoelectric application.

IV. CONCLUSION

$SrZnSb_2$ was found to be a heavily doped, small band gap semiconductor with *p*-type conduction. Low values of the electrical resistivity and Seebeck coefficient were observed, and a maximum zT of 0.30 was estimated for optimum doping at 500 K from a single, parabolic band model. A relatively low lattice thermal conductivity was observed ($\sim 1.2\ \mathrm{W\ m^{-1}\ K^{-1}}$ at room temperature), and the thermal transport was compared to that of the layered AZn_2Sb_2 ($A=\mathrm{Sr,Ca,Yb,Eu}$) compounds which have larger κ_L at moderate T. The main source for lower κ_L in $SrZnSb_2$ is likely to arise from the smaller density of acoustic modes, which is caused by the increased number of atoms per unit cell. Therefore, this work suggests that the number of atoms per unit cell should be considered when selecting layered Zintl compounds for investigation as potential thermoelectric materials.

ACKNOWLEDGMENTS

The Beckman Foundation is thanked for financial support.

[1] E. S. Toberer, C. A. Cox, S. R. Brown, T. Ikeda, A. F. May, S. M. Kauzlarich, and G. J. Snyder, Adv. Funct. Mater. **18**, 2795 (2008).
[2] A. F. May, J.-P. Fleurial, and G. J. Snyder, Phys. Rev. B **78**, 125205 (2008).
[3] X.-J. Wang, M.-B. Tang, J.-T. Zhao, H.-H. Chen, and X.-X. Yang, Appl. Phys. Lett. **90**, 232107 (2007).
[4] S.-J. Kim, S. Hu, C. Uher, and M. G. Kanatzidis, Chem. Mater. **11**, 3154 (1999).
[5] S.-J. Kim, S. Hu, C. Uher, T. Hogan, B. Huang, J. D. Corbett, and M. G. Kanatzidis, J. Solid State Chem. **153**, 321 (1999).
[6] E. S. Toberer and G. J. Snyder, Nature Mater. **7**, 105 (2008).
[7] G. K. H. Madsen, J. Am. Chem. Soc. **128**, 12140 (2006).
[8] F. Gascoin, S. Ottensmann, D. Stark, S. M. Haile, and G. J. Snyder, Adv. Funct. Mater. **15**, 1860 (2005).
[9] H. Zhang, J.-T. Zhao, Y. Grin, X.-J. Wang, M.-B. Tang, Z.-Y. Man, H.-H. Chen, and X.-X. Yang, J. Chem. Phys. **129**, 164713 (2008).
[10] J. K. Burdett and G. J. Miller, Chem. Mater. **2**, 12 (1990).
[11] H. J. Goldsmid and J. W. Sharp, J. Electron. Mater. **28**, 869 (1999).
[12] H. J. Goldsmid, *Applications of Thermoelectricity* (Butler & Tanner Ltd., London, 1960).
[13] E. S. Toberer, A. F. May, B. C. Melot, E. Flage-Larsen, and G. J. Snyder, in preparation.
[14] J. R. Drabble and H. J. Goldsmid, *Thermal Conduction in Semiconductors* (Pergamon, New York, 1961).
[15] D. G. Cahill, S. K. Watson, and R. O. Pohl, Phys. Rev. B **46**, 6131 (1992).
[16] E. Brechtel, G. Cordier, and H. Schaefer, Z. Naturforsch. B **34**, 251 (1979).
[17] A. Mewis, Z. Naturforsch. B **33**, 382 (1978).
[18] G. A. Slack and V. G. Tsoukala, J. Appl. Phys. **76**, 1665 (1994).
[19] G. A. Slack, *Solid State Physics* (Academic, New York, 1979), Vol. 34.
[20] G. P. Srivastava, Phys. Status Solidi B **90**, K125 (1978).
[21] J. M. Ziman, Philos. Mag. **1**, 191 (1956).
[22] J. M. Ziman, Philos. Mag. **2**, 292 (1957).
[23] L. R. Testardi, J. Appl. Phys. **32**, 1978 (1961).